http://dx.doi.org/10.1097/mm9.0000000000000046

MedMat

Original Research

OPEN

Magnetically driven microscavengers for microplastic degradation in blood

Jie Gao[a], Huaijuan Zhou[a,*], Song Li[a], Yingting Yang[a], Pei Li[b], Wei Qiao[c], Bahareh Khezri[d], Sijin Chen[e], Jinhua Li[f,*]

Abstract

Microplastics can traverse human physiological barriers, infiltrate and accumulate in critical organs and tissues (e.g., brain, blood, and heart) over extended periods, posing significant threats to human health. While microplastic degradation in aquatic environments (e.g., contaminated water) has been extensively studied, research on bloodstream microplastic degradation remains largely unexplored, leaving a critical gap in remediation strategies. To fill this gap, we pioneered the fabrication of biocompatible magnetically driven Fe_3O_4@polydopamine (PDA)-lipase microrobots by functionalizing Fe_3O_4 nanoparticles with PDA and lipase for blood-borne microplastic degradation. In vitro blood experiments confirmed that this platform holds promise for future detoxification of circulating microplastics. The microrobots integrate synergistic functions: Fe_3O_4 enables magnetic responsiveness for precise movement control; PDA provides adhesive properties for robust microplastic binding; and lipase mediates enzymatic microplastic degradation. Guided by an external rotating magnetic field, the microrobots achieve targeted microplastic capture and in situ enzymatic degradation in blood without releasing harmful substances, addressing a pivotal safety concern for biomedical applications. Performance evaluations showed ~25% microplastic degradation efficiency in blood after 7 days of incubation. Additionally, the microrobots can be effectively recycled via magnetic separation postdegradation, reducing residuals and improving practicality. Hemolysis assays using rabbit blood and toxicity evaluations using human umbilical vein endothelial cells and immunofluorescence experiments confirmed their excellent biocompatibility and immunogenicity, an indispensable prerequisite for potential in vivo translation. As a proof-of-concept study, this work provides a promising biocompatible approach for blood microplastic degradation and clearance, simultaneously overcoming the technical challenge of blood-specific targeted degradation and meeting safety requirements, thus laying a foundation for microrobot-based mitigation of microplastic health hazards.

Keywords: Enzymatic degradation, Magnetic navigation, Micro/nanorobots, Microplastics

1. Introduction

With the widespread application of plastic products in industrial production and daily life, microplastics—defined as plastic particles, fibers, and fragments with a diameter smaller than 5 mm[1]—have evolved into ubiquitous environmental contaminants, posing an escalating threat to both ecological integrity and human health[2]. Mounting evidence has documented the extensive distribution of microplastics in marine and freshwater systems, where they not only induce severe physiological damage to aquatic organisms but also disrupt the stability of marine food webs and the entire aquatic ecological system[3]. Beyond aquatic habitats, the long-term and large-scale use of plastic products has facilitated the pervasive dissemination of microplastic fragments into terrestrial environments (e.g., air and soil)[4]. Notably, nondegradable and difficult-to-degrade microplastics can enter living organisms (including humans) through multiple pathways: primarily via the food chain, as well as direct ingestion of plastic-packaged food or beverages (e.g., snacks and bottled water). Once internalized, microplastics are transported to multiple organs—even throughout the entire body—via blood circulation, accumulating in tissues such as the brain[5], heart[6], lungs[7], blood[8], and even blood clots[9]. These accumulations disrupt normal physiological functions, impair bone health[10], interfere with spermatogenesis and mitochondrial activity[11], trigger cardiovascular diseases and neurodegenerative disorders[12], and may even act as carriers to transport harmful substances (e.g.,

[a]School of Materials Science and Engineering, School of Interdisciplinary Science, Beijing Institute of Technology, Beijing, China, [b]Center for Advanced Biotechnology and Medicine, Rutgers University, Piscataway, New Jersey, USA, [c]Applied Oral Sciences and Community Dental Cares, Faculty of Dentistry, The University of Hong Kong, Hong Kong, China, [d]Inorganic and Physical Chemistry Department, Universitat Rovira i Virgili, Tarragona, Spain, [e]School of Life Science, Beijing Institute of Technology, Beijing, China, [f]Key Laboratory of Medical Molecule Science and Pharmaceutical Engineering, Ministry of Industry and Information Technology, Beijing Key Laboratory of Intelligent Molecular Materials and High-throughput Manufacturing, School of Chemistry and Chemical Engineering, Beijing Institute of Technology, Beijing, China.

*Corresponding authors: Address: Huaijuan Zhou, School of Materials Science and Engineering, School of Interdisciplinary Science, Beijing Institute of Technology, Beijing 100081, China. E-mail address: huaijuan.zhou@bit.edu.cn (H. Zhou); Jinhua Li, Key Laboratory of Medical Molecule Science and Pharmaceutical Engineering, Ministry of Industry and Information Technology, Beijing Key Laboratory of Intelligent Molecular Materials and High-throughput Manufacturing, School of Chemistry and Chemical Engineering, Beijing Institute of Technology, Beijing, 100081, China E-mail address: lijinhua@bit.edu.cn (J. Li).

Supplemental Digital Content is available for this article.

MedMat (2026) 3:2

Copyright © 2026 The Authors. Published by Wolters Kluwer Health, Inc. This is an open access article distributed under the Creative Commons Attribution License 4.0 (CCBY), which permits unrestricted use, distribution, and reproduction in any medium, provided the original work is properly cited.

Received: 2 November 2025; Accepted 22 March 2026

Published online 5 January 2026

viruses), thereby imposing profound and far-reaching threats to human health. Against this backdrop, the development of efficient strategies for in vivo microplastic removal and degradation has become an imperative research priority[13].

Currently, common microplastic removal methods (e.g., photocatalysis, gravity filtration, and coagulation) suffer from low efficiency, which is attributed to factors such as coagulant specificity, microplastic degradation resistance, and large equipment footprint[14]. Moreover, these methods often fail to achieve complete microplastic removal, resulting in residual contaminants in the environment. It is worth emphasizing that traditional wastewater treatment technologies are inherently unsuitable for in vivo microplastic degradation scenarios due to their lack of biocompatibility and precise targeting capability. In recent years, micro/nanorobots have emerged as a promising alternative for addressing environmental microplastic pollution, outperforming traditional technologies by virtue of their unique size effects and precise maneuverability[15]. Representative examples include (1) photocatalytic Au@Ni@TiO_2 micromotors, which can either attract and collect microplastics by generating localized chemical gradients or fluid flow via photocatalytic reactions, or directly propel and remove microplastics through the shovel effect of microchains under magnetic fields[16]; (2) magnetic algae robots (MARs), which achieve efficient microplastic capture and removal via magnetically driven active motion and electrostatic interactions between the negatively charged algal surfaces and positively charged microplastics[17]; and (3) keratin magnetic micro/nanorobots (KMNRs), which realize precise motion control via external magnetic fields—leveraging the magnetic actuation capability of Fe_3O_4 microspheres to boost kinetic adsorption efficiency and achieve highly efficient microplastic sequestration through synergistic physicochemical interactions, including electrostatic attraction toward microplastics and the abundant functional groups anchored on keratin fiber surfaces[18]. Despite these advances, existing micro/nanorobots exhibit inherent limitations: MARs are hampered by poor environmental adaptability and high cultivation costs; KMNRs suffer from low mechanical strength and susceptibility to changes in water physicochemical properties; and photocatalytic Au@Ni@TiO_2 micromotors are constrained by their reliance on ultraviolet light sources and potential metal ion leaching contamination. More crucially, these micro/nanorobots remain incompatible with the stringent benchmarks required for in vivo biomedical applications across 3 core dimensions: material biosafety, physiological microenvironment adaptability, and biodegradability. From a biosafety perspective, the intrinsic components or surface functional modifications of these micro/nanorobots may trigger unintended cytotoxicity, immune responses, or systemic inflammation when exposed to living tissues. In terms of physiological adaptability, the complex in vivo milieu—characterized by dynamic pH fluctuations, enzymatic degradation, and shear stress from blood flow or interstitial fluid—can disrupt the structural integrity and motion controllability of the robots, undermining their functional stability. Regarding biodegradability, nondegradable or slowly degrading micro/nanorobots are prone to accumulation in vital organs (e.g., liver and kidneys) over time, posing latent risks of chronic tissue damage. In sharp contrast, their current design and performance make them well-suited for environmental remediation scenarios, where they can be deployed to target and degrade microplastics in relatively open systems such as water bodies without strict constraints on biocompatibility.

In parallel with the development of environmental micro/nanorobots, numerous biomedical micro/nanorobots have been engineered for the detection, prevention, and treatment of various human diseases[19–26]. Building on this, we developed a novel magnetic Fe_3O_4@PDA-lipase microrobot platform by functionalizing Fe_3O_4 nanoparticles with PDA and lipase, specifically tailored for the capture and degradation of microplastics in blood (Figure 1).

This design integrates 3 core functional advantages: (1) the biocompatibility and magnetic responsiveness of Fe_3O_4 nanoparticles, enabling remote, precise motion control, and magnetic cycling via external magnetic fields; (2) the biocompatibility and strong adhesion performance of PDA, facilitating efficient microplastic capture; and (3) the enzymatic catalysis capability of lipase, realizing targeted microplastic degradation in physiological environments. To validate the performance of this microrobot platform, polycaprolactone (PCL) microplastics in 3 forms (particles, thin films, and microspheres) were used as model contaminants. Under the manipulation of external rotating magnetic fields, Fe_3O_4@PDA-lipase microrobots can actively approach and capture microplastics via PDA-mediated adhesion, degrade the captured microplastics through lipase-catalyzed hydrolysis

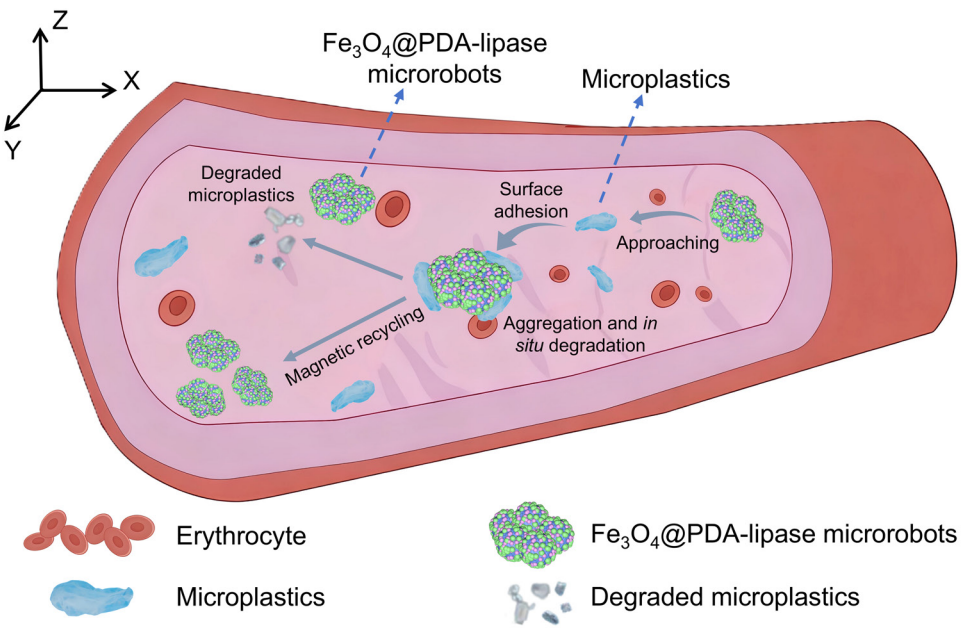

Figure 1. Schematic illustration of magnetically driven Fe_3O_4@PDA-lipase microrobots for microplastic capture and in situ enzymatic degradation in blood, with the microrobots enabling reuse via magnetic recycling.

in blood (using rabbit blood as the experimental matrix), and finally be completely retrieved from the blood via magnetic separation. As a pioneering micro/nanorobotic platform for blood-borne microplastic degradation, this work establishes a critical technical paradigm for removing microplastics in the bloodstream. More importantly, it addresses the long-standing gap between existing micro/nanorobots (which are only suitable for environmental remediation) and the urgent clinical demand for in vivo microplastic elimination, paving the way for the development of next-generation biomedical micro/nanorobots targeting internal microplastic pollution.

2. Experimental

2.1 Materials and reagents

All reagents were commercially available and used without further purification. Fe_3O_4, dichloromethane (CH_2Cl_2), and lipase (from porcine pancreas, 15~35 units/mg) were purchased from Aladdin. Dopamine hydrochloride and Tris(hydroxymethyl) aminomethane (Tris-HCl, pH 7.4) were purchased from Adamas-Beta. PCL and polyvinyl alcohol (PVA) were purchased from Sigma-Aldrich and Sigma, respectively. Polystyrene (PS) films were purchased from Taobao. Heparin sodium anticoagulant rabbit blood was obtained from Nanjing SenBeiJia Biological Technology Co., Ltd. Phosphate buffer saline (PBS, pH 7.2–7.4), human umbilical vein endothelial cells (HUVECs), and cell counting kit-8 (CCK-8) were purchased from Adamas-Life. Calcein-AM/propidium iodide cell viability/cytotoxicity assay kit (Calcein-AM/PI) was purchased from Beyotime, while human brain vascular endothelial cells complete medium (HBVECs CM; composition: basic culture medium 1×, serum 5%, cell growth factors, double resistant) was purchased from Keycell. Notably, PCL was used after undergoing specific pretreatment, which is introduced in section 2.5. Tohoku Hospital Pediatrics-1 (THP-1) cells were purchased from FuHeng in Shanghai. 4′,6-diamidino-2-phenylindole was purchased from Medchemexpress. NF-κB p65 Polyclonal antibody and Nano-Secondary anti-human IgG/anti-rabbit IgG VHHs were purchased from Proteintech. Lipopolysaccharide (LPS) was purchased from Solarbio.

2.2 Characterization

The crystal structure of the materials was characterized by X-ray diffraction (XRD, Malvern Panalytical-X'Pert, Netherlands) while their magnetic properties were evaluated using a vibrating sample magnetometer (VSM, Lakeshore-7404, USA). The infrared spectra of samples were recorded via attenuated total reflection Fourier transform infrared spectroscopy (ATR-FTIR, Thermo Fisher Scientific IS5, USA), and their morphology was observed by scanning electron microscopy (SEM, Hitachi S-4800, Japan). The elemental changes of materials were characterized by energy dispersive spectroscopy (EDS, Oxford, England). Additionally, the movement behaviors of microrobots were observed using an Eclipse Ts2 inverted fluorescence microscope (Nikon, Japan) with a built-in CCD camera.

2.3 Preparation of Fe_3O_4@PDA-lipase microrobots

First, 40 mg of commercially purchased Fe_3O_4 nanoparticles were ultrasonically dispersed in 20 mL of Tris solution, and the pH of the mixture was adjusted to 8.5 using 0.1 M NaOH solution. Then, 40 mg of dopamine hydrochloride was ultrasonically dissolved into the above Fe_3O_4-Tris solution, resulting in a final concentration of 20 mg/mL for both Fe_3O_4 nanoparticles and dopamine hydrochloride. The mixed solution was placed on a shaker at room temperature and shaken at 99 rpm overnight to induce the self-polymerization of dopamine hydrochloride, yielding the Fe_3O_4@PDA solution. The as-prepared Fe_3O_4@PDA solution was washed twice and then dried in an oven at 60 °C to obtain a powder. Subsequently, this powder was ultrasonically dispersed in PBS containing lipase at a concentration of 12.5 mg/mL, followed by incubation at room temperature overnight. After washing and drying treatment, Fe_3O_4@PDA-lipase microrobots were obtained due to the electrostatic interaction between lipase and Fe_3O_4@PDA[27].

2.4 Magnetic actuation and motion performance characterization of microrobots

A permanent magnet with dimensions of 15 cm × 10 cm × 5 cm and a steady magnetic flux density (B) of 0.3 T was employed as the dedicated magnetic actuation source to provide controllable external magnetic fields for the Fe_3O_4@PDA-lipase microrobots. This magnet was rigidly mounted on a programmable robotic arm, with its magnetic field direction aligned parallel to the X-axis of the experimental coordinate system. The robotic arm was programmed to drive the magnet to perform axial rotation around the X-axis at a constant angular velocity of 100 r/min, thereby generating a rotating magnetic field to manipulate the directional motion of the target microrobots. As schematically illustrated in Supplementary Figure S1, https://links.lww.com/MEDMAT/A10, the robotic arm executed counterclockwise rotation about the X-axis when observed from the positive X-axis (X+) to the negative X-axis (X–) direction, a configuration designed to ensure consistent torque transmission to the microrobots in the liquid medium.

For quantitative characterization of microrobot locomotion behavior, the dynamic motion of the microrobots in deionized (DI) water and in vitro blood matrices was real-time monitored using an inverted optical microscope equipped with a high-speed camera. The acquired microscopic image sequences were imported into *ImageJ* software for postprocessing analysis, where the morphological size and spatial displacement of the microrobots at different time intervals were precisely measured. To guarantee the reliability and statistical significance of the experimental data and the consistency of experimental conditions, 3 particles of each size were selected from the same video for calculation. The final reported results are expressed as the mean value with the corresponding standard deviation.

2.5 Preparation of PCL powder, film, and microsphere

PCL was prepared into 3 morphologies (powder, film, and microspheres) following the procedures below:

For PCL powder, bulk PCL was directly ground into a powder.

For PCL films, first, 400 mg of bulk PCL was fully dissolved in 5 mL of dichloromethane (CH_2Cl_2). The resulting solution was then dropped into a glass dish, which was rotated rapidly to form a uniform film. Subsequently, the glass dish was dried in an oven at 40 °C to ensure complete evaporation of CH_2Cl_2. Finally, the film was peeled off with a spatula and cut to the required weight and size.

For PCL microspheres, initially, 400 mg of bulk PCL was fully dissolved in 5 mL of CH_2Cl_2. Then, 2.5 mL PVA solution (50 mg/mL) was added to the PCL-CH_2Cl_2 mixture; the combined solution was vortexed for 1 min and ultrasonicated for 2 min. Finally, this solution was transferred to a PVA solution and stirred continuously to facilitate solvent volatilization and microsphere solidification[28].

2.6 Degradation of PCL microplastics

Degradation experiments of PCL powder and microspheres, as well as PS films, were implemented following the protocols detailed below.

2.6.1 Degradation assay of PCL films

PCL films were randomly divided into experimental groups and blank control groups, with 3 parallel replicates set for each group to ensure the reliability of experimental data. For experimental groups, individual PCL films were accurately weighed using an analytical balance to record the initial dry weight (W_0). Subsequently, the films were immersed in 2 degradation media: (1) DI water and (2) in vitro blood, both supplemented with a predetermined concentration of Fe_3O_4@PDA-lipase microrobots. The reaction systems were incubated in a constant-temperature shaking incubator at 37 °C (simulating physiological temperature) with a shaking speed of 120 rpm to ensure uniform contact between the microrobots and the film surfaces. At preset time intervals (1, 2, 3, 4, 5, and 7 days), the PCL films were carefully collected from the media. The retrieved films were rinsed thoroughly with DI water to remove residual microrobots and matrix components, then transferred to a vacuum drying oven at 50 °C and dried to a constant weight (W_t). After drying, the macroscopic morphology of the degraded films was documented using a digital camera, and the degradation efficiency (DE) was calculated according to the formula:

$$DE(\%) = \frac{W_0 - W_t}{W_0} \times 100\%, \quad (1)$$

For blank control groups, PCL films were subjected to the identical immersion, incubation, sampling, washing, and drying procedures in DI water and in vitro blood without the addition of Fe_3O_4@PDA-lipase microrobots.

2.6.2 Degradation assay of PS films

The degradation experiments of PS films were performed following the identical protocols applied to the PCL film degradation assay, including the grouping strategy, incubation conditions, sampling time points, and efficiency calculation method. This consistent experimental design ensured the comparability of degradation performance between PCL and PS films.

2.6.3 Degradation assay of PCL powder and microspheres

PCL microspheres were dispersed in *in vitro* blood containing Fe_3O_4@PDA-lipase microrobots respectively. The mixed system was incubated at 37 °C in a constant-temperature incubator for a total degradation period of 5 days. After degradation, the PCL powder and microspheres were separated from the medium via centrifugation (3000 rpm, 5 min), rinsed sequentially with DI water and ethanol to remove adsorbed microrobots and protein impurities, and then dried at 50 °C in a vacuum drying oven. Finally, SEM and ATR-FTIR tests were conducted on PCL powder and microspheres before and after degradation.

2.7 Cyclic degradation performance test

To evaluate the reusability and catalytic stability of Fe_3O_4@PDA-lipase microrobots, cyclic degradation experiments of PCL films were conducted following the completion of the first 5-day degradation cycle, with each cycle strictly controlled for consistency in reaction conditions. Upon the conclusion of the first degradation cycle, a permanent magnet was placed adjacent to the reaction vessel to achieve rapid, targeted adsorption of the Fe_3O_4@PDA-lipase microrobots via magnetic separation. The supernatant was carefully decanted to remove residual degradation products and unreacted matrix components. Subsequently, the collected microrobots underwent a systematic purification process: they were alternately rinsed with anhydrous ethanol and DI water for 3 cycles (5 min per rinse) to eliminate adsorbed PCL degradation fragments, protein impurities (from blood), and other contaminants. After washing, the microrobots were transferred to a constant-temperature oven set at 37 °C and dried to a constant weight to avoid moisture interference with subsequent catalytic activity.

The regenerated Fe_3O_4@PDA-lipase microrobots were then redeployed to initiate a new round of PCL film degradation under identical experimental conditions (37 °C incubation temperature, same reaction medium volume, and similar initial weight of PCL film). Each degradation cycle was standardized to a duration of 5 days. To comprehensively assess the long-term performance of the microrobots, this adsorption–washing–regeneration–degradation cycle was repeated for 4 consecutive rounds, with the DE of PCL films recorded for each cycle.

2.8 Hemolysis assay

The hemolytic potential of Fe_3O_4@PDA-lipase microrobots was evaluated following a standardized protocol[29] with 3 parallel replicates set for each experimental group to ensure data reliability. Fresh rabbit blood was first diluted 10-fold with sterile phosphate-buffered saline (PBS, pH 7.4) to prepare a red blood cell (RBC) suspension, which was then mixed thoroughly with Fe_3O_4@PDA-lipase microrobots at a series of gradient concentrations (e.g., 10, 20, 30, and 40 μg/mL). Sterile PBS and DI water were used as the negative control (no hemolysis) and positive control (complete hemolysis), respectively. All mixtures were incubated in a constant-temperature oven at 37 °C for 4 h, followed by centrifugation at 3000 rpm for 5 min to precipitate intact RBCs and cellular debris. Subsequently, 200 μL of the supernatant from each sample was carefully transferred to a 96-well microplate, and the optical density (OD) value of released hemoglobin was measured at a wavelength of 540 nm using a microplate reader. The hemolysis ratio (HR) of each sample was calculated according to Equation 2:

$$\mathrm{HR} = \frac{\mathrm{OD(Sample)} - \mathrm{OD(Neg)}}{\mathrm{OD(Pos)} - \mathrm{OD(Neg)}}, \quad (2)$$

2.9 Quantitative cell viability evaluation

HUVECs were cultured in HBVEC-conditioned medium in a cell culture incubator (CCI) at 37 °C with 5% CO_2. Cells were seeded into a 96-well culture plate at a density of 8×10^3 cells per well. Once cell confluency reached 80%, they were incubated with Fe_3O_4@PDA-lipase microrobots at various concentrations for 24 h. The negative control was treated with PBS (without Fe_3O_4@PDA-lipase microrobots), and the blank control group contained only medium (without cells). After removing the co-culture mixture, 100 μL of diluted CCK-8 solution was added to each well. The 96-well plate was then returned to the CCI for a 3-h incubation. Subsequently, 100 μL of supernatant from each well was transferred to a new 96-well plate. Finally, the OD of the supernatant was measured at 450 nm using a microplate reader, and the cell viability of each sample was calculated according to Equation 3.

$$\mathrm{Cell\,viability} = \frac{\mathrm{OD_{Sample}} - \mathrm{OD_{Blank\,Control}}}{\mathrm{OD_{Negative\,Sample}} - \mathrm{OD_{Blank\,Control}}}, \quad (3)$$

2.10 Qualitative cell viability evaluation

Cell viability and cytotoxicity of Fe_3O_4@PDA-lipase microrobots were qualitatively assessed via dual fluorescent staining with Calcein-AM and Propidium Iodide (PI). HUVECs in the logarithmic growth phase were seeded into the 48-well plates at a density of 1.5×10^4 cells per well and cultured under standard conditions (37 °C, 5% CO_2) until the cell confluency reached 80%. The original medium was then replaced with fresh complete medium containing Fe_3O_4@PDA-lipase

microrobots at gradient concentrations (20 and 40 μg/mL), while cells incubated with complete medium without microrobots served as the control group. After a 24 h co-incubation, the culture medium was aspirated completely, and the cells were rinsed once with precooled sterile PBS to remove residual microrobots and nonadherent cells. Subsequently, 150 μL of working Calcein-AM/PI staining solution (final concentrations: Calcein-AM and PI were 1 × in detection buffer) was added to each well, and the 48-well plate was sealed with parafilm to prevent evaporation and incubated in a CO_2 incubator for 30 min under dark conditions to avoid fluorescence quenching. Finally, cell morphology and fluorescence staining patterns were observed and imaged using an inverted fluorescence microscope (Eclipse Ts2, Nikon, Japan), where live cells exhibited green fluorescence (intact cell membrane and active esterase activity) and dead cells exhibited red fluorescence (damaged cell membrane).

2.11 Immunofluorescence

The THP-1 cells were seeded into a 24-well plate (2×10^4 cells per well). When the cell density reached 70%, the cells were incubated with different concentrations of Fe_3O_4@PDA-lipase microrobots and LPS for 12 h. The untreated group served as the negative control, while the LPS-treated positive drug stimulation group acted as the positive control. After washing away free microrobots with PBS, cells were stained according to the manufacturer's protocol. Observations were made under an inverted fluorescence microscope (Eclipse Ts2, Nikon, Japan).

3 Results and discussion

3.1 Synthesis and characterization of Fe_3O_4@PDA-lipase microrobots

First, a uniform biomimetic adhesive PDA layer was constructed on the surface of Fe_3O_4 nanoparticles via a self-polymerization method using mild synthesis conditions. Subsequently, lipase was efficiently immobilized onto this layer via electrostatic interactions to fabricate Fe_3O_4@PDA-lipase microrobots (Figure 2A). XRD patterns showed that the diffraction peaks of Fe_3O_4@PDA and Fe_3O_4@PDA-lipase microrobots were highly consistent with those of pristine Fe_3O_4, indicating no significant changes in the crystal structure (Figure 2B)[30]. VSM was used to evaluate the magnetic properties of Fe_3O_4 nanoparticles and Fe_3O_4@PDA-lipase microrobots. VSM curves confirmed that the magnetic property profile remains unchanged. However, the saturation magnetization decreased from 57.6 to 45.4 emu/g due to the presence of PDA and lipase (Figure 2C). Nevertheless, Fe_3O_4@PDA-lipase microrobots still maintained good responsiveness to external magnetic fields and could be attracted by a magnet (inset in Figure 2C). ATR-FTIR and EDS were further used to confirm the successful immobilization of PDA and lipase on Fe_3O_4 nanoparticles. For Fe_3O_4@PDA-lipase microrobots, the ATR-FTIR spectrum showed that the Fe-O bond peak persisted but was narrower, indicating the magnetic core remained intact. Additionally, significant changes occurred in the peaks at 3400, 1650, and 1540 cm^{-1}. The broadened peak at 3400 cm^{-1} resulted from the overlap of O-H and N-H stretching vibrations (from the phenolic hydroxyl and amino groups of PDA), the peak at 1650 cm^{-1} (amide I) corresponded to the C=O stretching vibration of the

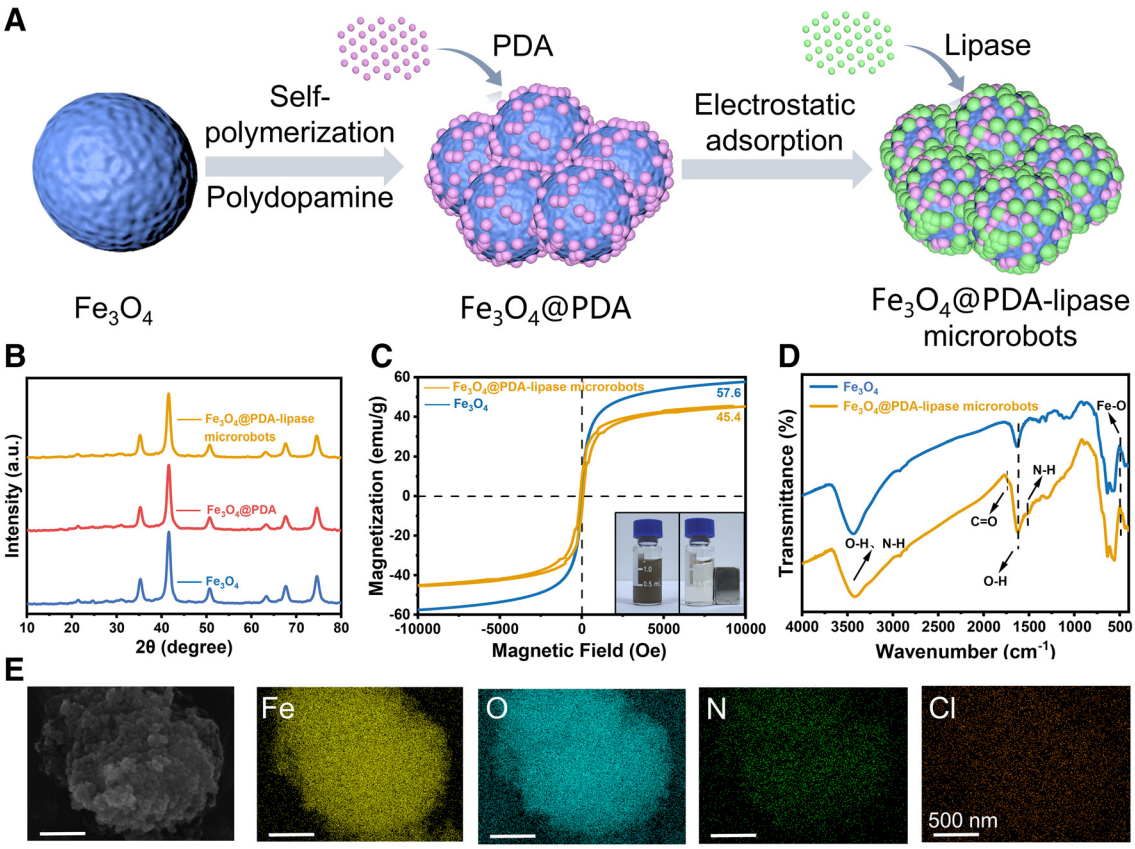

Figure 2. Synthesis and characterization of the Fe_3O_4@PDA-lipase microrobots. (A) Schematic illustration of the synthesis process of Fe_3O_4@PDA-lipase microrobots. (B) XRD patterns of Fe_3O_4, Fe_3O_4@PDA, and Fe_3O_4@PDA-lipase microrobots. (C) VSM curves. (D) ATR-FTIR spectra. (E) SEM image of Fe_3O_4@PDA-lipase microrobots and corresponding EDS element mapping of the elements Fe, O, N, and Cl.

lipase backbone (with enhanced intensity due to the overlap with C=C vibrations of PDA), and the peak at 1540 cm^{-1} (amide II) originated from the coupling of N-H bending and C-N stretching vibrations (Figure 2D)[10]. EDS further confirmed the presence of characteristic elements (Fe, O, N, and Cl) in Fe_3O_4@PDA-lipase microrobots, and morphological observation revealed the microrobots exhibited a relatively regular, uniform spherical structure (Figure 2E, Supplementary Figure S2, https://links.lww.com/MEDMAT/A11). Collectively, these results demonstrate that PDA and lipase were successfully grafted onto the surface of Fe_3O_4 nanoparticles, enabling the fabrication of Fe_3O_4@PDA-lipase microrobots.

3.2 Motion performance of Fe_3O_4@PDA-lipase microrobots

The magnetically guided orientation movement of Fe_3O_4@PDA-lipase microrobots was realized by rotating a magnet at a constant speed via a mechanical robotic arm, which generated a uniform magnetic field. As our previous research has demonstrated, the velocity of micro/nanorobots is strongly associated with their particle sizes[27]. To investigate the motion characteristics of Fe_3O_4@PDA-lipase microrobots, experiments were conducted on microrobots with dimensions of 5, 15, 25, 35, and 45 μm. Under the identical conditions, the velocities of Fe_3O_4@PDA-lipase microrobots in water and blood showed a close relation with their particle sizes. Thus, it can be concluded that the size of the microrobots was a crucial factor in determining their motion speed. This phenomenon is attributed to the fact that larger microrobots traverse a longer distance in response to an external magnetic field during a single flip cycle. Specifically, as blood contains a higher proportion of red blood cells, white blood cells and platelets, coupled with the influence of hemodynamic forces, the velocities of Fe_3O_4@PDA-lipase microrobots in water were greater than those in blood (Figure 3A, B)[31]. When the robotic arm started rotating, Fe_3O_4@PDA-lipase microrobots underwent regular flipping motion within the XOY plane along the magnetic field direction, with distinct directionality in their flipping process. Specifically, the particles completed symmetric flipping using magnetic field lines as the reference axis, and the entire motion process was stable and could be precisely regulated via external parameters (Figure 3C and Video 1).

3.3 Microplastic capture in the blood

Owing to the excellent super-adhesive properties of PDA[32], Fe_3O_4@PDA-lipase microrobots inherently possess the ability to adsorb PCL microplastics in blood. Under the guidance of external magnetic fields, these microrobots then move synchronously with the adsorbed PCL microplastics. This coordinated motion is critical as it ensures sustained contact between the robots and the target substrate, thereby effectively promoting the enzymatic degradation of PCL. After the degradation cycle, Fe_3O_4@PDA-lipase microrobots can be efficiently retrieved by precisely regulating the magnetic field parameters (e.g., intensity and direction). This recoverability is a key advantage for practical applications, as it enables the microrobots to be reused in successive adsorption-degradation cycles, significantly improving the cost-effectiveness and sustainability of the system (Figure 4A). Experiments on PCL's cyclic degradation also confirmed the reusability of Fe_3O_4@PDA-lipase microrobots (Supplementary Figure S3, https://links.lww.com/MEDMAT/A12). In the case where the same batch of Fe_3O_4@PDA-lipase microrobots underwent 3 recycling processes, PCL films still exhibited DEs of 23.6% and 16.3% in water and blood, respectively. To systematically verify the reliable magnetic control capability of Fe_3O_4@PDA-lipase microrobots in the complex blood environment, a validation experiment was designed: Fe_3O_4@PDA-lipase microrobots and PCL microplastics were coincubated in a blood-filled culture dish for real-time observation. Initially, by precisely adjusting the magnetic field direction, the microrobots were successfully driven to migrate toward PCL microplastics, demonstrating accurate target-tracking ability (0–6 s). Once contacting PCL plastics, the magnetic field was maintained to keep the Fe_3O_4@PDA-lipase microrobots upward while they adhered tightly to the PCL surface (6–17 s), confirming the robustness of PDA-mediated adhesion even during dynamic motion. Subsequently, reversing the magnetic field direction caused the microrobots to carry the adsorbed PCL and move downward together, further validating that the magnetic control signal could overcome the resistance from the blood matrix and maintain the integrity of the microrobots-PCL complex (17–25 s) (Figure 4B and Video 2). These results clearly indicate that even in a complex blood matrix, Fe_3O_4@PDA-lipase microrobots can stably adsorb PCL microplastics and move synchronously with them, exhibiting excellent magnetic drive capability.

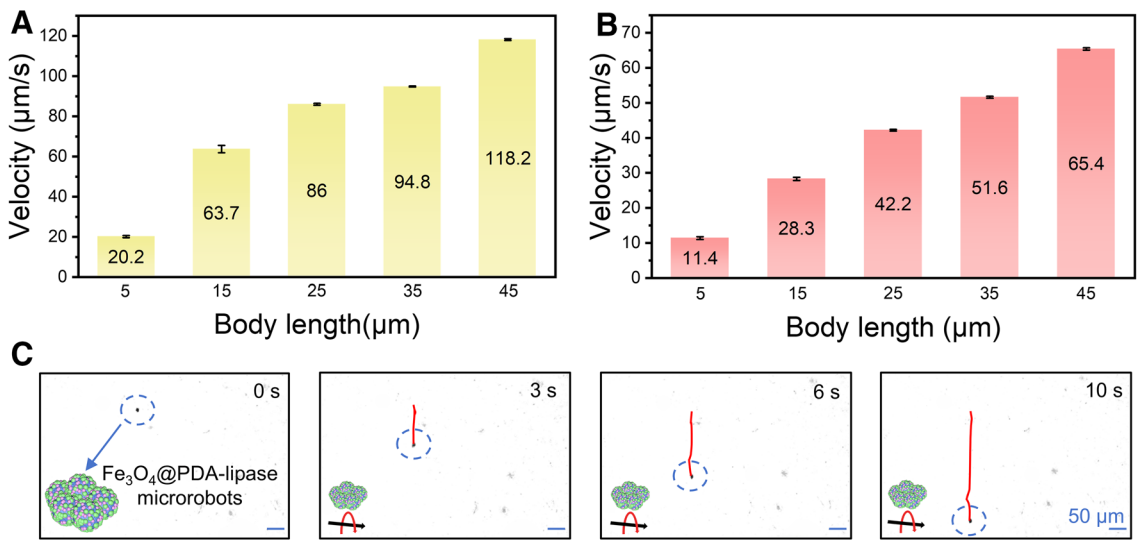

Figure 3. Motion performance of Fe_3O_4@PDA-lipase microrobots. (A) Velocity of Fe_3O_4@PDA-lipase microrobots in water. (B) Velocity of Fe_3O_4@PDA-lipase microrobots in blood. (C) Time-lapse tracking images of Fe_3O_4@PDA-lipase microrobots in blood.

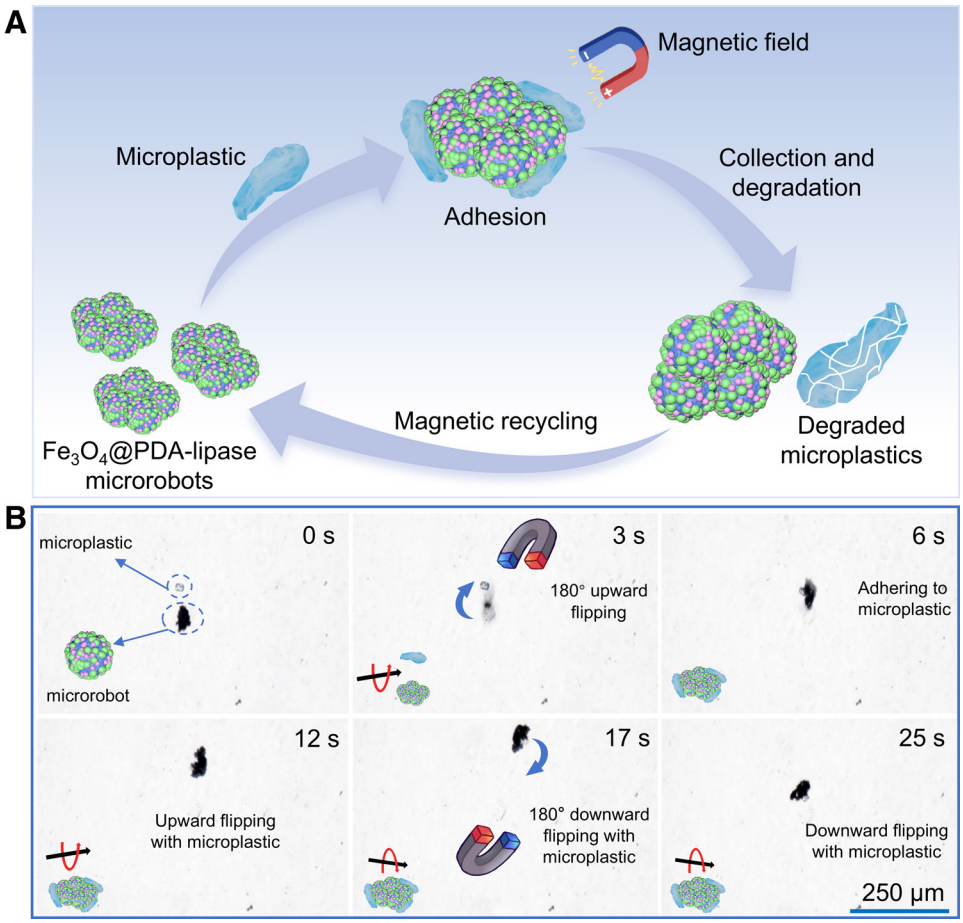

Figure 4. The adsorption and removal of PCL microplastics by Fe_3O_4@PDA-lipase microrobots in blood. (A) Action mechanism of Fe_3O_4@PDA-lipase microrobots in blood. (B) Time-lapse tracking images of magnetically driven motion of Fe_3O_4@PDA-lipase microrobots for approaching and adhering to PCL microplastics in blood.

3.4 Microplastic degradation

To confirm that Fe_3O_4@PDA-lipase microrobots maintain effective degradation performance in complex physiological environments, their DE on PCL plastics was evaluated. Here, PCL in the form of a thin film was used. Experimental results showed that PCL films underwent significant degradation in both water and blood, driven by the synergy of hydrolysis and enzymatic digestion[33]—a dual-degradation mechanism that mimics the combined chemical action and biological processes in the in vivo milieu. The DE of PCL films showed a steady upward trend. Notably, blood has a lower water content than pure water[34], which relatively inhibited PCL hydrolysis and directly resulted in lower DE of PCL films in blood compared with DI water. Quantitative analysis further validated this difference: after 7 days, the DE of PCL films reached 39.1% in water, while it was only 25.3% in blood. Compared with the blank group, the presence of microrobots significantly enhanced the DE of PCL (Figure 5A, B). From a morphological perspective, the degradation process of PCL films in blood exhibited distinct stage-specific characteristics: within 2 days, slight degradation occurred, causing intact films to fragment. The formation of cracks not only increased the specific surface area of PCL exposed to degradation agents (e.g., water molecules and enzymes) but also created new channels for these agents to penetrate the film's internal structure. As a result, by days 4 and 7, PCL film fragmentation became more prominent, with films gradually breaking down into smaller fragments (Figure 5C). A similar staged degradation pattern was also observed in water, further confirming the universality of the Fe_3O_4@PDA-lipase microrobots' degradation mechanism (Supplementary Figure S4, https://links.lww.com/MEDMAT/A13).

To further verify the substrate specificity of lipase-mediated catalytic degradation, we additionally conducted parallel control experiments utilizing PS plastic films—a representative polymer substrate devoid of ester bonds[35]. Under the identical experimental conditions (37 °C incubation temperature, 7-day reaction duration, and consistent microrobot concentration) applied to PCL films, the PS films exhibited negligible DE (less than 5%), with no observable changes in macroscopic morphology or weight loss (Supplementary Figure S5, https://links.lww.com/MEDMAT/A14, and Supplementary Figure S6, https://links.lww.com/MEDMAT/A15). These comparative experimental results unambiguously validated the intrinsic substrate specificity of lipase, which exclusively catalyzes the hydrolysis of ester linkages rather than acting on the carbon-carbon backbone structures of non-ester-containing polymers such as PS[36,37]. Collectively, these findings underscore the precise catalytic mechanism of the Fe_3O_4@PDA-lipase microrobotic system. Notably, as a versatile and modular platform for microplastic degradation, this microrobotic system enables the flexible substitution of lipase with other substrate-specific enzymes tailored to the chemical structures of diverse microplastics (e.g., cutinase for polyethylene terephthalate (PET) degradation[38], protease for protein-based biodegradable plastics[39]). This customizable design confers the system with robust adaptability and holds immense potential for the targeted remediation of complex microplastic-contaminated environments in future practical applications.

To better analyze and observe microplastic degradation, PCL powder was placed in blood at 37 °C for degradation using the

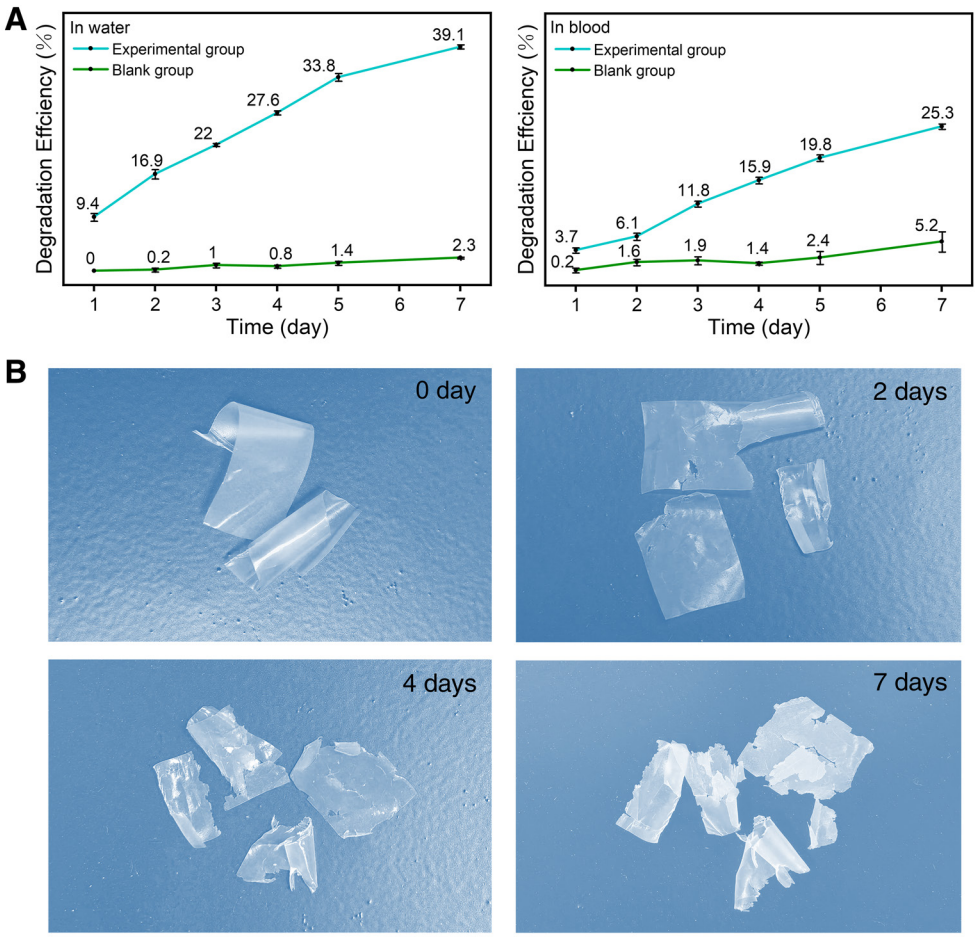

Figure 5. Degradation of PCL films in water and blood. (A) Degradation efficiency of PCL films in water for 7 days cocultured with and without Fe_3O_4@PDA-lipase microrobots. (B) Degradation efficiency of PCL films in blood for 7 days cocultured with and without Fe_3O_4@PDA-lipase microrobots. (C) Macroscopic morphology evolution of PCL films after degradation with Fe_3O_4@PDA-lipase microrobots in blood for 2, 4, and 7 days.

same method. On day 5, the powder was collected, washed, and dried. Changes in their ATR-FTIR peaks after degradation were analyzed by comparing with the pre-degradation spectrum. Before degradation, PCL powder showed a sharp, intense peak at 1730 cm^{-1} (attributed to the carbonyl stretching vibration in ester groups), and characteristic asymmetric/symmetric C-H stretching peaks at 2945 and 2866 cm^{-1}, respectively[40]. After hydrolysis and enzymatic degradation, the characteristic peaks of carbonyl and C-H bond significantly weakened. In contrast, a broader and more intense peak appeared near 3438 cm^{-1} in the degraded PCL powder, which originated from O-H stretching vibration in the newly formed terminal hydroxyl and carboxyl groups (from hydrolysis). With ester bond cleavage, the peak at 1170 cm^{-1} (assigned to C-O-C asymmetric stretching vibration) also showed a marked intensity decrease (Figure 6A)[41]. SEM was further used to observe changes in the surface morphology of PCL microspheres. After 5 days of degradation, the microsphere surface exhibited increased erosion and roughness, with larger pits forming and pores becoming more prominent (Figure 6B)[42]. These results confirm that PCL microspheres undergo chemical degradation through enzymatic reaction.

3.5 Biocompatibility tests of Fe_3O_4@PDA-lipase microrobots

To assess the degradation capacity of Fe_3O_4@PDA-lipase microrobots in blood, their blood compatibility, which is critical for preventing hemolysis, was first evaluated, as red blood cell rupture-induced hemolysis poses serious risks to biological systems[43]. When incubated with rabbit blood, the hemolysis rate of Fe_3O_4@PDA-lipase microrobots was below 5%, which meets the standards specified in ISO 10993-4 (Figure 7A)[44]. In addition to blood compatibility, cellular compatibility is equally essential. HUVECs, a widely used model for evaluating vascular biocompatibility due to their relevance to physiological environments, were selected as the test cells. Preliminary cytotoxicity assessments of Fe_3O_4@PDA-lipase microrobots at various concentrations showed that HUVEC viability remained above 80% (Figure 7B), confirming good cellular biocompatibility[45]. To further verify the microrobots' impact on cell viability, a cell viability/cytotoxicity assay was conducted. After 24 h of coculture with HUVECs, only minimal red fluorescence (indicating dead cells) was detected (Figure 7C), directly demonstrating that Fe_3O_4@PDA-lipase microrobots exert negligible adverse effects on cell viability. Collectively, these results confirm that magnetically driven Fe_3O_4@PDA-lipase microrobots exhibit excellent biocompatibility.

3.6 Immunogenicity tests of Fe_3O_4@PDA-lipase microrobots

Immunofluorescence staining was employed to assess the effect of different treatment regimens on NF-κB p65 nuclear translocation in THP-1 cells. In the negative control group (untreated

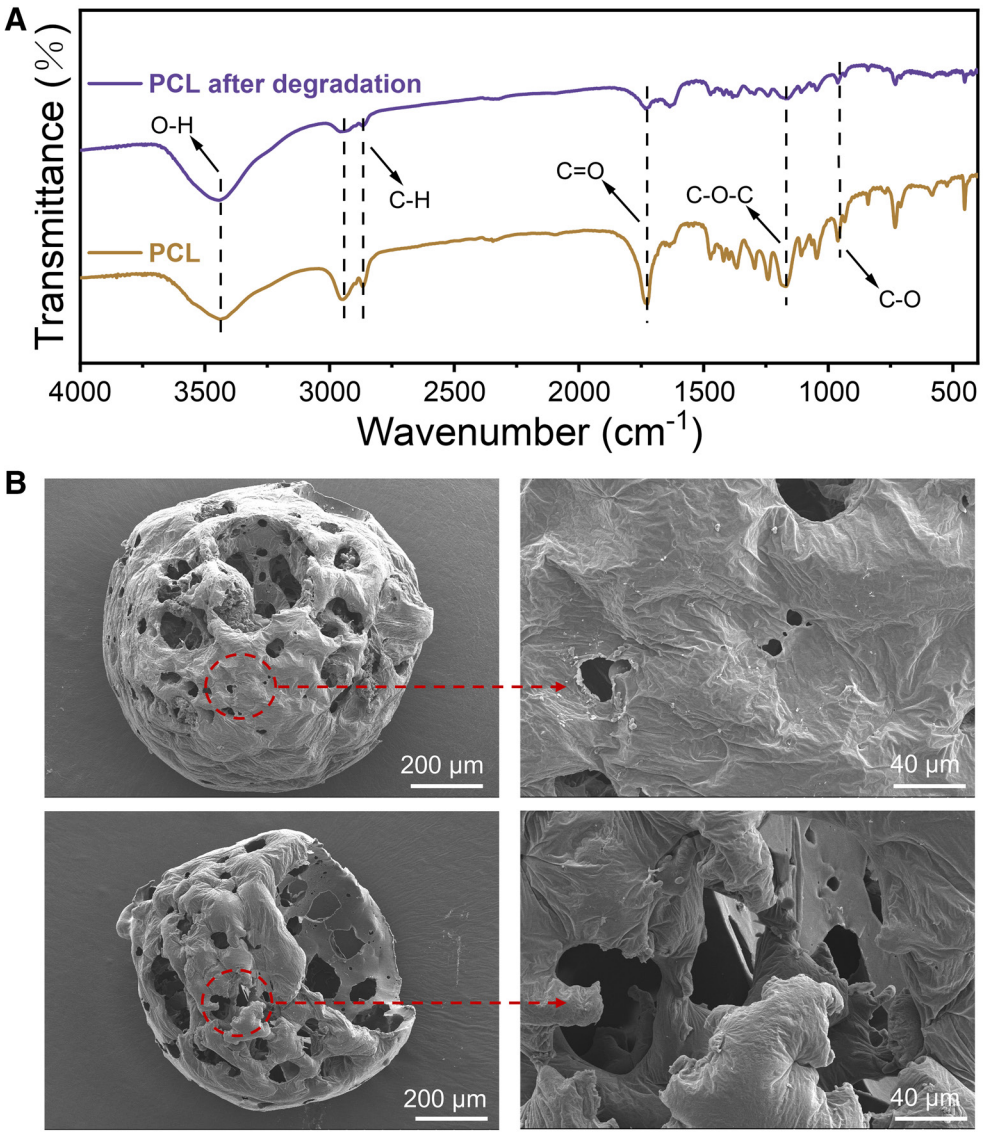

Figure 6. Degradation of PCL microspheres in blood. (A) ATR-FTIR images of PCL microspheres before and after degradation in blood for 5 days. (B) SEM images of the microstructure of PCL microspheres before and after 5 days of degradation in blood.

cells), p65 was predominantly localized in the cytoplasm, with negligible nuclear fluorescence signals. In contrast, the positive control group (12-h LPS stimulation) exhibited marked NF-κB p65 nuclear translocation, accompanied by a significant enhancement in nuclear fluorescence intensity. For the experimental groups (THP-1 cells treated with 10, 20, 30, and 40 μg/mL Fe_3O_4@PDA-lipase microrobots for 12 h), the extent of p65 nuclear translocation was intermediate between that of the negative and positive control groups. While faint nuclear fluorescence signals were detected in a subset of cells in the experimental groups, p65 remained predominantly cytoplasmic in the majority of cells (Figure 8, Supplementary Figure S7, https://links.lww.com/MEDMAT/A16). These findings demonstrate that Fe_3O_4@PDA-lipase microrobots induce mild NF-κB p65 nuclear translocation in THP-1 cells, with the activation level being markedly lower than that triggered by LPS stimulation. This weak activation profile confirms the low immunogenicity of Fe_3O_4@PDA-lipase microrobots, validating their potential as relatively safe biomaterials for biological applications.

4. Conclusions

In summary, we developed multifunctional Fe_3O_4@PDA-lipase microrobots with promising potential for targeted degradation of microplastics in blood. This system integrates 3 core functionalities—magnetic navigation (from Fe_3O_4), microplastic adhering (via PDA), and enzymatic hydrolysis (by lipase)—into a single platform, enabling a closed-loop process of targeting, capturing, degrading microplastics, and facilitating the microrobots' recovery for reuse, followed by safe clearance of degraded products. Under external magnetic fields, the Fe_3O_4@PDA-lipase microscavengers exhibit rotational motion; they adhere to PCL particles while moving in blood, thereby enhancing DE, achieving a 25% microplastic degradation within 7 days. Moreover, the microrobots can be precisely retrieved via magnetic field regulation for repeated reuse cycles. Furthermore, the microrobots demonstrate efficacy across diverse environments and excellent biosafety (validated by hemolysis assays, cytotoxicity evaluations, and immunogenicity experiments). These features, coupled with their capacity to

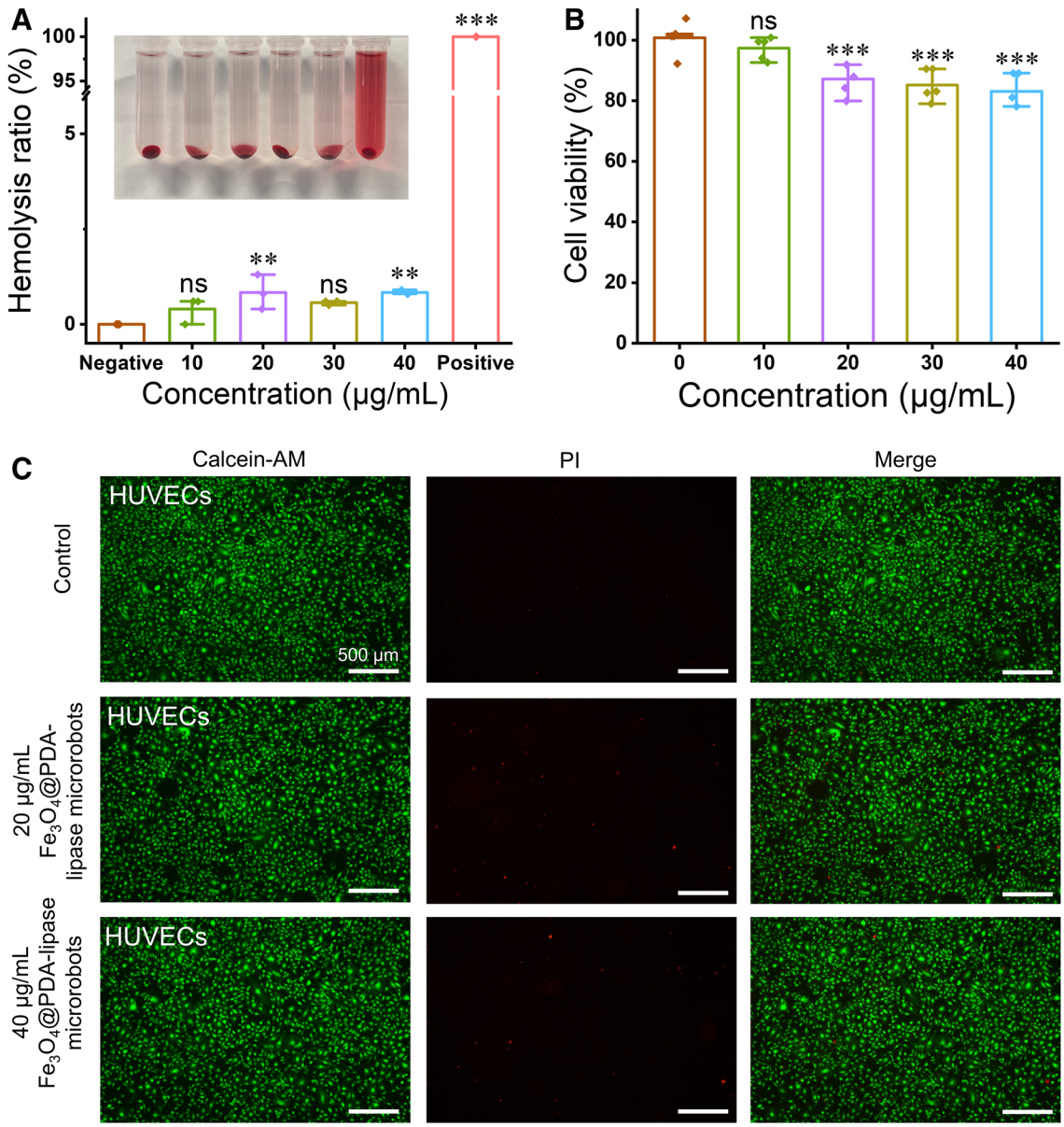

Figure 7. Biosafety evaluation. (A) Hemolysis rates of Fe_3O_4@PDA-lipase microrobots at different concentrations. (B) HUVEC viability after 24 h of coculture with Fe_3O_4@PDA-lipase microrobots. (C) fluorescence images of HUVECs stained with Calcein-AM (labeling live cells, green fluorescence) and PI (labeling dead cells, red fluorescence) after treatment with Fe_3O_4@PDA-lipase microrobots for 24 h. Statistical differences between groups were analyzed using one-way ANOVA (**$P \leq 0.01$ and ***$P \leq 0.001$). Each group was compared with the negative control group or blank group.

traverse physiological barriers, underscore the great application potential of these magnetically driven microrobots as a novel, controllable, and sustainable strategy for in vivo microplastic remediation—with their utility extending beyond blood to cerebrospinal fluid and other physiological niches.

Acknowledgments

This work was financially supported by the Beijing Natural Science Foundation (Grant No. 2242059).

Conflicts of interest

The authors declare that they have no conflicts of interest.

Data availability statement

The data are available from the corresponding author upon reasonable request.

Author contributions

Jie Gao: Investigation, formal analysis, data curation, visualization, writing–original draft. Huaijuan Zhou: conceptualization, funding acquisition, project administration, supervision, writing–review & editing. Song Li, Yingting Yang, Pei Li, Wei Qiao, Bahareh Khezri, and Sijin Chen: investigation, validation. Jinhua Li: conceptualization, resources, supervision, writing – review & editing. All authors discussed and approved the final manuscript.

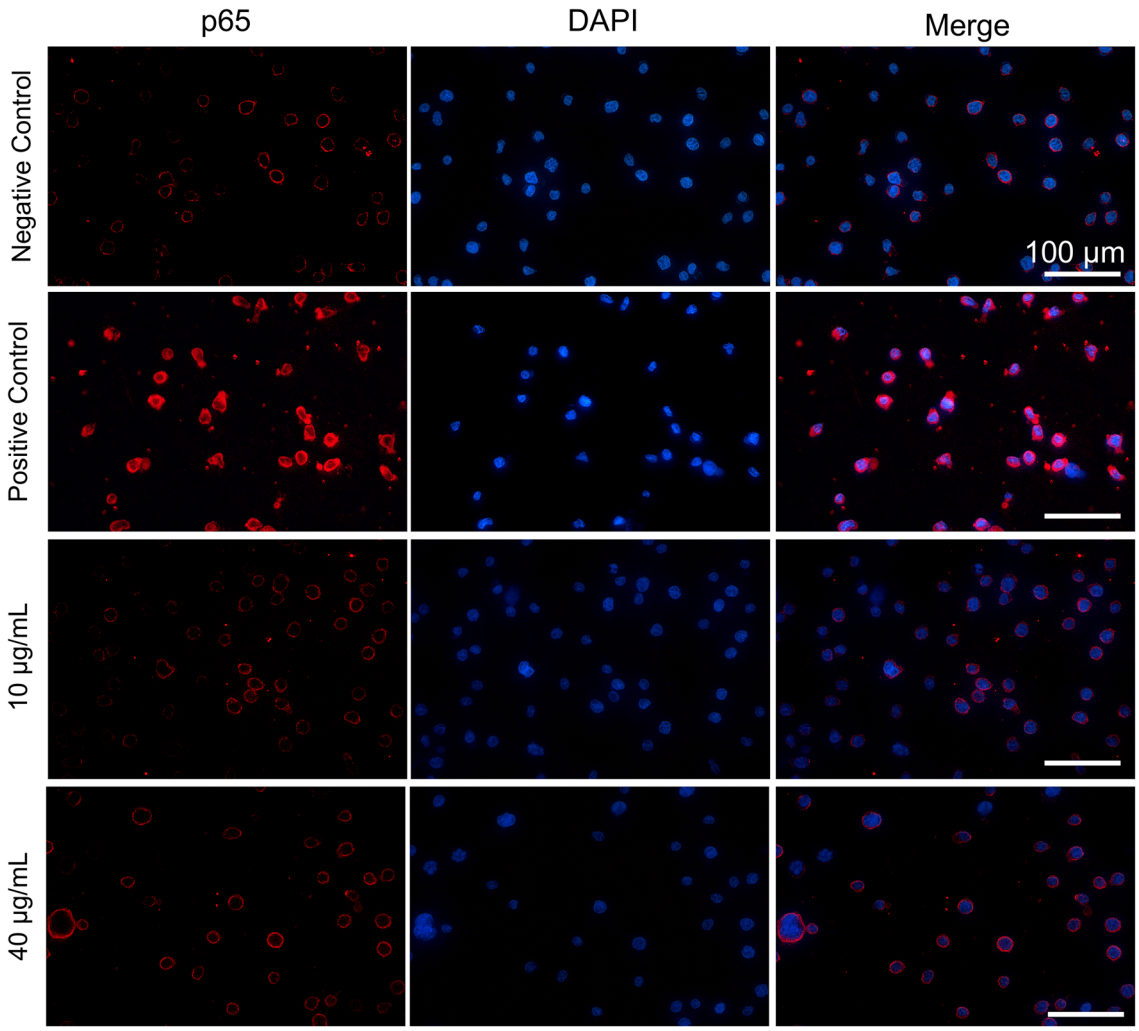

Figure 8. Immunofluorescence staining images of the negative control group, 10 and 40 μg/mL Fe_3O_4@PDA-lipase microrobot-treated groups, and the LPS-stimulated positive control group.

References

[1] Allen D, Allen S, Abbasi S, et al. Microplastics and nanoplastics in the marine-atmosphere environment. *Nat Rev Earth Environ*. 2022;3(6):393–405.

[2] Thompson RC, Olsen Y, Mitchell RP, et al. Lost at sea: where is all the plastic? *Science*. 2004;304(5672):838–838.

[3] Auta HS, Emenike CU, Fauziah SH. Distribution and importance of microplastics in the marine environment: a review of the sources, fate, effects, and potential solutions. *Environ Int*. 2017;102:165–176.

[4] Huang W, Xia X. Element cycling with micro(nano)plastics. *Science*. 2024;385(6712):933–935.

[5] Nihart AJ, Garcia MA, El Hayek E, et al. Bioaccumulation of microplastics in decedent human brains. *Nat Med*. 2025;31(4):1114–1119.

[6] Yang Y, Xie E, Du Z, et al. Detection of various microplastics in patients undergoing cardiac surgery. *Environ Sci Technol*. 2023;57(30):10911–10918.

[7] Amato-Lourenço LF, Carvalho-Oliveira R, Júnior GR, et al. Presence of airborne microplastics in human lung tissue. *J Hazard Mater*. 2021;416:126124.

[8] Leslie HA, van Velzen MJM, Brandsma SH, et al. Discovery and quantification of plastic particle pollution in human blood. *Environ Int*. 2022;163:107199.

[9] Wu D, Feng Y, Wang R, et al. Pigment microparticles and microplastics found in human thrombi based on Raman spectral evidence. *J Adv Res*. 2023;49:141–150.

[10] Zhang Y-W, Zhou D-Y, Wang S-C, et al. Bridging relevance between microplastics, human health and bone metabolism: emerging threats and research directions. *Environ Chem Ecotoxicol*. 2024;6:422–435.

[11] Zhao Q, Fang Z, Wang P, et al. Polylactic acid micro/nanoplastic exposure induces male reproductive toxicity by disrupting spermatogenesis and mitochondrial dysfunction in mice. *ACS Nano*. 2025;19(5):5589–5603.

[12] Liu Z, Sokratian A, Duda AM, et al. Anionic nanoplastic contaminants promote Parkinson's disease–associated α-synuclein aggregation. *Sci Adv*. 2023;9(46):eadi8716.

[13] Zhou H, Yang Y, Li P, et al. Micro/nanorobots for the removal of microplastics and nanoplastics from the human body. *Med Mat*. 2025;2(4):183–187.

[14] Mustapha S, Tijani JO, Elabor R, et al. Technological approaches for removal of microplastics and nanoplastics in the environment. *J Environ Chem Eng*. 2024;12(2):112084.

[15] Wu X, Peng X, Ren L, et al. Reconfigurable magnetic liquid metal microrobots: a regenerable solution for the capture and removal of micro/nanoplastics. *Adv Funct Mater*. 2024;34(51):2410167.

[16] Wang L, Kaeppler A, Fischer D, et al. Photocatalytic TiO2 micromotors for removal of microplastics and suspended matter. *ACS Appl Mater Interfaces*. 2019;11(36):32937–32944.

[17] Peng X, Urso M, Kolackova M, et al. Biohybrid magnetically driven microrobots for sustainable removal of micro/nanoplastics from the aquatic environment. *Adv Funct Mater*. 2024;34(3):2307477.

[18] Zhang M, Yang S, Zhong W, et al. Upscaling waste human hairs into micro/nanorobots for adsorptive removal of micro/nanoplastics. *Chem Eng J*. 2024;495:153264.

[19] Zhou H, Mayorga-Martinez CC, Pané S, et al. Magnetically driven micro and nanorobots. *Chem Rev*. 2021;121(8):4999–5041.

[20] Shi D, Wang X, Deng Y, et al. Smart micro/nanorobots for drug delivery in the brain. *Prog Mater Sci*. 2026;155:101533.

[21] Zhou H, Dong G, Gao G, et al. Hydrogel-based stimuli-responsive micromotors for biomedicine. *Cyborg Bionic Syst*. 2022;2022:9852853.
[22] Li S, Zhou H, Shi D, et al. Micro/nanorobots for detecting and eliminating biological and chemical warfare agents. *BMEMat*. 2025;4:e70021.
[23] Wang F, Zhang Y, Jin D, et al. Magnetic soft microrobot design for cell grasping and transportation. *Cyborg Bionic Syst*. 2024;5:0109.
[24] Li J, Dekanovsky L, Khezri B, et al. Biohybrid micro- and nanorobots for intelligent drug delivery. *Cyborg Bionic Syst*. 2022;2022:9824057.
[25] Sun Z, Hou Y. Intelligent micro/nanorobots for improved tumor therapy. *BMEMat*. 2023;1(2):e12012.
[26] Wang T, Chen Z, Huang Q, et al. Advanced microrobots driven by acoustic and magnetic fields for biomedical applications. *Cyborg Bionic Syst*. 2025;6:0386.
[27] Zhou H, Mayorga-Martinez CC, Pumera M. Microplastic removal and degradation by mussel-inspired adhesive magnetic/enzymatic microrobots. *Small Methods*. 2021;5(9):e2100230.
[28] Kemala T, Budianto E, Soegiyono B. Preparation and characterization of microspheres based on blend of poly(lactic acid) and poly(ε-caprolactone) with poly(vinyl alcohol) as emulsifier. *Arabian J Chem*. 2012;5(1):103–108.
[29] You J, Liu S, Liang J, et al. Adaptive dual-responsive nanocapsules for precision ferroptosis-driven and chemotherapy-enhanced tumor ablation. *MedMat*. 2024;1(2):104–117.
[30] Fu X, Sarker S, Ma W, et al. Novel phenylalanine-modified magnetic ferroferric oxide nanoparticles for ciprofloxacin removal from aqueous solution. *J Colloid Interface Sci*. 2023;632:345–356.
[31] Lovegrove JT, Kent B, Förster S, et al. The flow of anisotropic nanoparticles in solution and in blood. *Exploration (Beijing)*. 2023;3(6):20220075.
[32] Tsai W-B, Chen W-T, Chien H-W, et al. Poly(dopamine) coating to biodegradable polymers for bone tissue engineering. *J Biomater Appl*. 2014;28(6):837–848.
[33] Bartnikowski M, Dargaville TR, Ivanovski S, et al. Degradation mechanisms of polycaprolactone in the context of chemistry, geometry and environment. *Prog Polym Sci*. 2019;96:1–20.
[34] Benga G, Matei H, Borza T, et al. Comparative nuclear magnetic resonance studies of diffusional water permeability of red blood cells from different species. V--Rabbit (Oryctolagus cuniculus). *Comp Biochem Physiol B*. 1993;106(2):281–285.
[35] Hwang J, Choi D, Han S, et al. Potential toxicity of polystyrene microplastic particles. *Sci Rep*. 2020;10(1):7391.
[36] Liu M, Zhang T, Long L, et al. Efficient enzymatic degradation of poly (ε-caprolactone) by an engineered bifunctional lipase-cutinase. *Polym Degrad Stab*. 2019;160:120–125.
[37] Pastorino L, Pioli F, Zilli M, et al. Lipase-catalyzed degradation of poly(ε-caprolactone). *Enzyme Microb Technol*. 2004;35(4):321–326.
[38] Akram E, Cao Y, Xing H, et al. On the temperature dependence of enzymatic degradation of poly(ethylene terephthalate). *Chin J Catal*. 2024;60:284–293.
[39] Cao Y, Ma W, Chen S, et al. Immobilization of proteinase K into PLA for self-biodegradable. *Int J Biol Macromol*. 2025;304:140873.
[40] Khan I, Ray Dutta J, Ganesan R. Lactobacillus sps. lipase mediated poly (ε-caprolactone) degradation. *Int J Biol Macromol*. 2017;95:126–131.
[41] Yeingst TJ, Arrizabalaga JH, Rawnaque FS, et al. Controlled degradation of polycaprolactone polymers through ultrasound stimulation. *ACS Appl Mater Interfaces*. 2023;15(29):34607–34616.
[42] Lu B, Wang G-X, Huang D, et al. Comparison of PCL degradation in different aquatic environments: effects of bacteria and inorganic salts. *Polym Degrad Stab*. 2018;150:133–139.
[43] Zhao R, Liu X, Yang X, et al. Artificial organelles: nanomaterial-based organelles protect normal cells against chemotherapy-induced cytotoxicity. *Adv Mater*. 2018;30(27):1801304.
[44] Geng H, Wang T, Cao H, et al. Antibacterial ability, cytocompatibility and hemocompatibility of fluorinated graphene. *Colloids Surf B Biointerfaces*. 2019;173:681–688.
[45] Novak M, Žegura B, Modic B, et al. Cytotoxicity and genotoxicity of anticancer drug residues and their mixtures in experimental model with zebrafish liver cells. *Sci Total Environ*. 2017;601-602:293–300.

How to cite this article: Gao J, Zhou H, Li S, Yang Y, Li P, Qiao W, Khezri B, Chen S, Li J. Magnetically driven microscavengers for microplastic degradation in blood. MedMat 2026;3(2):e00046. doi: 10.1097/mm9.0000000000000046